Applied Clay Science 50 (2010) 245–254

Contents lists available at ScienceDirect

Applied Clay Science

journal homepage: www.elsevier.com/locate/clay

Technological characterization and industrial application of two Turkish clays for the ceramic industry

H. Celik *

Usak University, Faculty of Fine Arts, Department of Ceramic, Bir Eylul Campus, Usak, Turkey

ARTICLE INFO

Article history:
Received 24 July 2009
Received in revised form 26 July 2010
Accepted 3 August 2010
Available online 13 August 2010

Keywords:
Clay mineral
Chemical and physical properties
Industry
Ceramic

ABSTRACT

This study focuses on the mineralogical, chemical, thermal and physical characterization of Afyon and Istanbul clays from Turkey and evaluation of the potential of the Afyon clay to manufacture traditional ceramic products with industrial processing. The suitability of the raw clay material from Afyon region to produce floor tiles was not tested yet. The effect of partial substitution of the clay from Istanbul–Sile deposit (one of the main clay producing areas of Turkey) by Afyon clay on ceramic properties was studied. The studied samples were kaolinite (Istanbul clay) and illite (Afyon clay) based materials. While there were no major differences in water absorption, the bending strength decreased slightly when the kaolinitic Istanbul clay was substituted by the illitic Afyon clay for floor tile production. Almost all technological properties of the Afyon clay deposit demonstrated the industrial suitability of Afyon clay as a potential ceramic raw material for the growing Turkish ceramic tile industry.

1. Introduction

Clays are used as raw materials in many industrial fields such as ceramics, paper, paint, petroleum industry, clarification of various effluents, catalysis, etc. (Chang, 2002). Their applications are tightly dependent on their structure, composition, and physical properties (Grim, 1960). Knowledge of these properties is important for understanding the technology of ceramic production and optimization of the firing cycles.

Ceramic tiles are composed essentially of clays and other inorganic raw materials such as quartz, feldspar, and carbonates. The clays are the most important material from the technological point of view. In the fabrication process, the raw materials are mixed taking into account the influence of each component on the properties of the final materials, followed by processing steps such as pressing and firing (Sousa and Holanda, 2005). Common components that play fundamental roles for optimum processing, and hence performance of the final products, are kaolins for plasticity, silica as filler, and feldspar as fluxing agent to lower the temperature required to form a vitreous phase that promotes densification (Kamseu et al., 2007).

The mineralogical composition of the clays influences plasticity. The type of the clay mineral and the particle size distribution as well as the quantity and type of accessory materials alter plasticity (de Modesto and Bernardin, 2008). Among the main impurities that possess non-plastic properties are iron minerals (mainly Fe_2O_3), aluminium oxide, sodic and potassium feldspars, soluble salts (K_2SO_4, NaCl, Na_2CO_3, etc.), calcium minerals (mainly calcite) and silica (Ancey, 2007; Peters, 1991). Atterberg classifies the soils according to their plasticity indices (PI), for non-plastic soils PI = 0, for low plastic soils PI < 7, for medium plastic soils PI between 7 and 17, and for highly plastic soils PI > 17 (Murthy, 2003).

According to the Ceramic Tile World Data Reports prepared by Turkish Ceramics Federation (TCF), Turkey is currently the sixth world-wide producer and the fifth world-wide exporter of ceramic floor and wall tiles. The evolution of the Turkish ceramic covering tile profiles is shown in Fig. 1. The Turkish ceramic covering tile industry presented a rapid growth since 1990. In 2006, Turkish ceramic tile industry grew around 440% with production of 280 million meter square as compared with production in 1990. In addition, the Turkish production can grow still more due to the high internal demand which increased by 325% in 2006 when compared with 1990 (TCF, 2009).

Turkish standard TS EN 14411 (2006) defines terms and establishes classifications, characteristics and marking requirements for ceramic tiles of the best commercial quality. Table 1 shows the classification of dry-pressed ceramic tiles according to their groups and their specific product standards.

The raw clay material from Afyon region was neither tested for floor tile production nor characterized. Thus, to investigate the suitability of this clay for manufacturing floor tile bodies is of interest from an academic and technological viewpoint. The objective of this work is to evaluate the viability of the Afyon clay deposit as an industrial mineral by comparing its mineralogical, chemical and thermal features as well as its physical, mechanical and fired properties with a known industrial clay taken as reference.

* Tel.: +90 276 263 41 95; fax: +90 276 263 41 96.
E-mail address: haluk.celik@usak.edu.tr.

0169-1317/$ – see front matter © 2010 Elsevier B.V. All rights reserved.
doi:10.1016/j.clay.2010.08.005

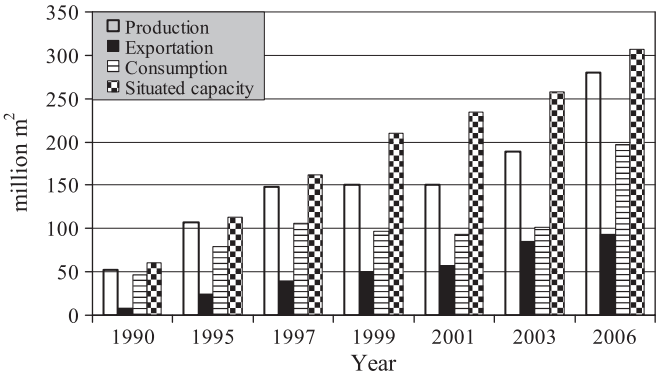

Fig. 1. Evolution of the Turkish ceramic covering tile industry profile.

2. Materials and methods

2.1. Material

The Afyon clay deposit is located about 5 km north of the town of Alanyurt, Afyon, in the Aegean Zone of Turkey. There is no previous work related to this material. The coordinates and location of AC deposit and geological map of the Turkey Toposheet No: J25-C4 on which AC mine area exist are given in Fig. 2. The mine area covers an area of approximately 50 ha as given in the toposheet at 1/25.000 scaled geology map (MTA, 2010). The Istanbul clay deposit is located near to town of Sile, about 68 km east of Istanbul, in the Marmara Zone of Turkey. The IC deposit is widely used as raw materials by ceramic plants in Turkey for the production of clay based structural ceramics. Total reserves (apparent and probable) are around 150 million tons for AC (Celik et al., 2009) and 279.4 million tons for IC as given MTA (2010) (General Directorate of Mineral Research and Exploration of Turkey) report of mineral resources of Istanbul provinces.

About twenty large samples (20 to 30 kg each) were collected directly from the Afyon deposit by digging a pit or using a hand auger in order to ensure a representative sample. They were blended thoroughly and then quartered into 1 kg aliquotes to provide statistically valid samples for laboratory assessment including characterization study and industrial processing tests. A sample of about 30 kg of the Istanbul–Sile clay was obtained from the stockpile of Hitit Ceramic Factory in Usak, Turkey, and quartered into about 1 kg aliquotes for laboratory studies. The 1-kg samples were dried at 110 °C for 24 h, manually crushed, and classified to particles <2000 μm.

2.2. Mineralogical and chemical analysis

The mineralogical analyses of the raw clay samples, as well as its corresponding clay fraction (<2 μm) were carried out by X-ray diffraction techniques (XRD). To obtain clay patterns more clearly for XRD analysis, the <2 μm clay fraction was separated from the raw clay samples by sedimentation, and centrifugation (Brindley and Brown, 1980). Small amounts of the clay–water dispersion were left to dry on glass slides to obtain oriented specimens. To provide additional information essential for the identification of clay minerals, the clays were examined after drying at room temperature, after reaction with ethyleneglycole for 1 h to detect expandable clay minerals and after heating to 550 °C for 3 h to differentiate chlorite and kaolinite (Thorez, 1975). The XRD patterns were obtained with a Rigaku Rint-2200 diffractometer operating at tube voltage and current 40 kV and 30 mA, respectively using monochromatic Cu-Kα_1 radiation ($\lambda = 1.5406$ Å). Diffraction patterns were recorded between 5 and70° 2θ with scanning rate of 2°/min. Quantification of different phases was carried out using the computer program MAUD 1.9 (Lutterotti, 2010), which is based on the Rietveld method combined with a Fourier analysis (Can et al., in Press). The chemical composition of the samples was determined by X-ray fluorescence (XRF) in a Spectro IQ equipment.

Table 1
Water absorption and bending strength requirements for dry-pressed ceramic tiles according to Turkish Standards TS EN 14411 (2006).

Dry-pressed ceramic tiles	Group	Water absorption (W_a), %	Bending strength, N/mm^2
With low water absorption	BI_a	$W_a \leq 0.5$ individual maximum 0.6	Minimum 35 individual minimum 32
	BI_b	$0.5 < W_a \leq 3$ individual maximum 3.3	Minimum 30 individual minimum 27
With moderate water absorption	BII_a	$3 < W_a \leq 6$ individual maximum 6.5	Minimum 22 individual minimum 20
	BII_b	$6 < W_a \leq 10$ individual maximum 3.3	Minimum 18 individual minimum 16
With high water absorption	BIII	$W_a > 10$ individual maximum 9	15 (thickness ≥ 7.5 mm) 12 (thickness < 7.5 mm)

2.3. Thermal analysis (DTA-TGA)

A differential calorimeter apparatus Netzsch STA 409 under air atmosphere was used for differential thermal analysis-thermo gravimetric analysis (DTA-TGA). The temperature was increased from room temperature to 1200 °C at a rate of 10 °C/min, kept at this maximum temperature for 10 min.

2.4. Dilatometry test

The firing characteristics of the raw clay samples were determined by heating the sample up to 1200 °C at a heating rate of 50 °C/min to 1100 °C, 30 °C/min for temperatures between 1100 and 1200 °C, and maintained at maximum temperature for 10 min. The pressed sample was dried overnight at 105 °C and then heated in the Misura 3.32 ODHT-HSM 1600/80 dilatometer. Length changes were recorded every minute during the heating stage.

2.5. Evaluation of plasticity

The evaluation of plasticity was performed by Atterberg limits method: liquid limit (LL), plastic limit (PL) and plasticity index (PI). The PI was calculated as the arithmetic difference of LL and PL. The LL and PL tests were carried out with a Casagrande apparatus using the method described by Casagrande (1947).

2.6. Particle size analysis

A combination of wet sieve screening for the fraction >125 μm and X-ray sedimentation technique for the fraction <125 μm was used. For the sieve screening, 100 g samples dispersed in deionised water were disaggregated using 0.1% sodium hexametaphosphate. For the X-ray sedimentation analysis, the <125 μm fraction (about 3 g) was disaggregated using 0.5% sodium hexametaphosphate, agitated mechanically and disaggregated ultrasonically. The size analysis was performed with the Mikromeritics SediGraph 5120 particle size analyzer, size range 0.1–300 μm.

2.7. Specific surface area and specific density

Quantachrome Autosorb-1C model surface analyzer was used for determining the specific surface areas by nitrogen adsorption (Brunauer et al., 1938). All samples were preliminary degassed under nitrogen at 300 °C for 1 h. The density was measured with a helium pycnometer (Quantachrome Multipycnometer).

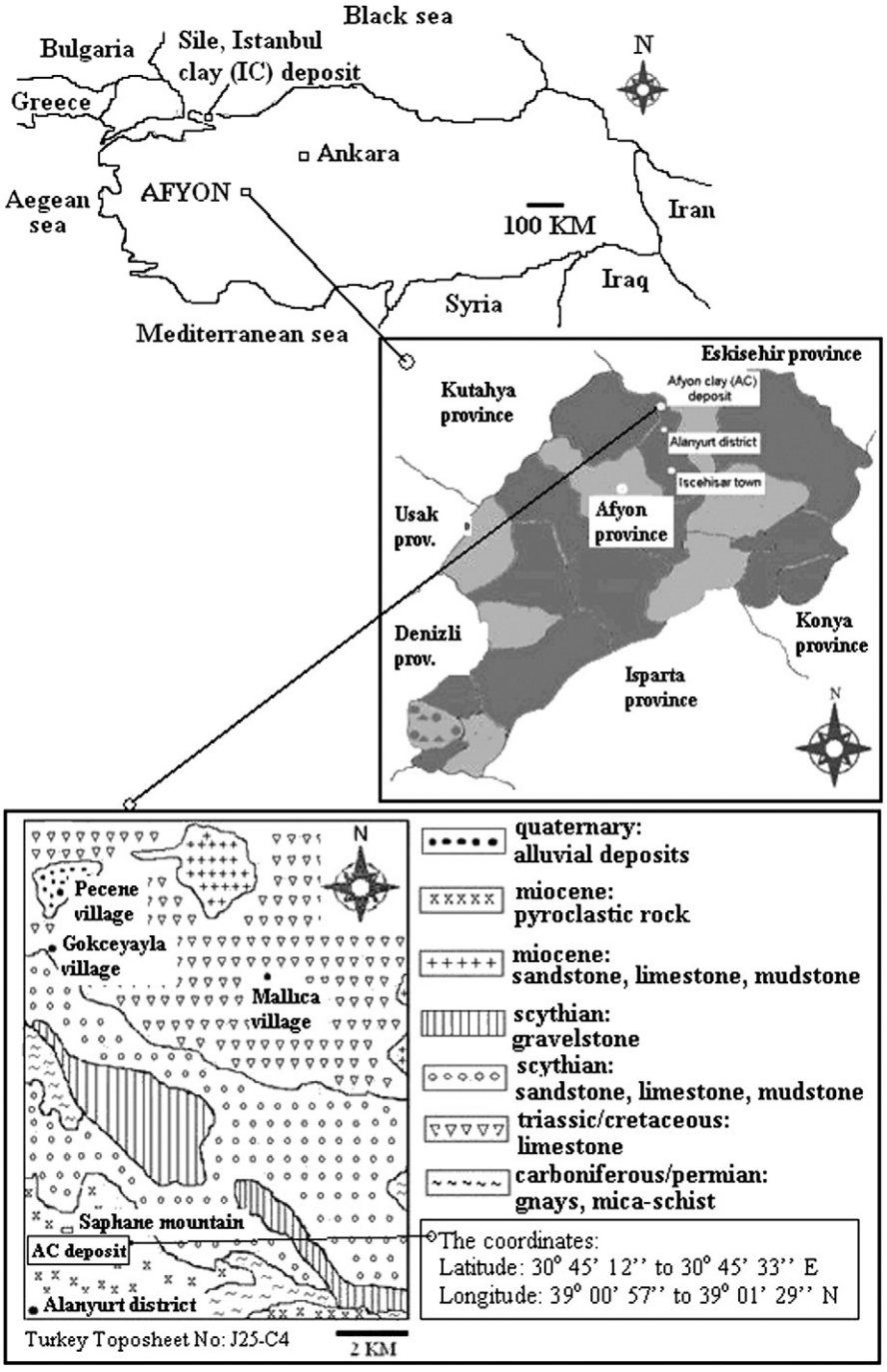

Fig. 2. Location and geological map of the Afyon clay deposit.

2.8. Industrial processing

The mixtures were ground using a jet mill and sieved <180 μm, the oversize fraction was recorded. After the measurement of the mass per liter with the pycnometer (100 cm^3) and viscosity by the Ford-cup (100 cm^3) of the <180 μm fraction, the sample was dried at 105 °C. It was ground to fine powder in a porcelain mortar and pestled with gentle vertical crushing movement for 30 min. The fine powder was humidified (6 mass% moisture content), homogenized and pressed at 250 kg/cm^2 giving specimens of $80\times35\times7$ mm^3 by the Gabbrielli Titan, Italy mark press. The shaped green specimens were dried at 110 °C for 24 h until constant mass was achieved. The dried bodies were characterized by the measurement of drying shrinkage and bending strength. The firing step was carried out in commercially kiln at the plant within firing cycle of total 33 min (cold-to-cold). During firing, the heating and cooling rates were kept at 80 °C/min and at 90 °C/min, respectively. The specimens were maintained at 1196 °C for 6 min. Firing characteristics (shrinkage, water absorption, and bending strength) were measured, and the colour of the fired bodies was classified in terms of *L*, *a* and *b* parameters. The formed minerals were identified by XRD.

The bending strength was carried out using the three-point bending test (Nannetti Faenza, Italy), and calculated by $3FL/2bh^2$ in which F = breaking load (kg), L = distance between supports (mm), b = sample with (mm) and h = sample thickness (mm). The dimensions of the pressed specimens were measured before and after firing to determine the firing shrinkage by $100(L_d - L_f)/L_d$, where L_d = the length of the dried specimen and L_f = the length of the fired specimen. The water absorption values were determined by the routine

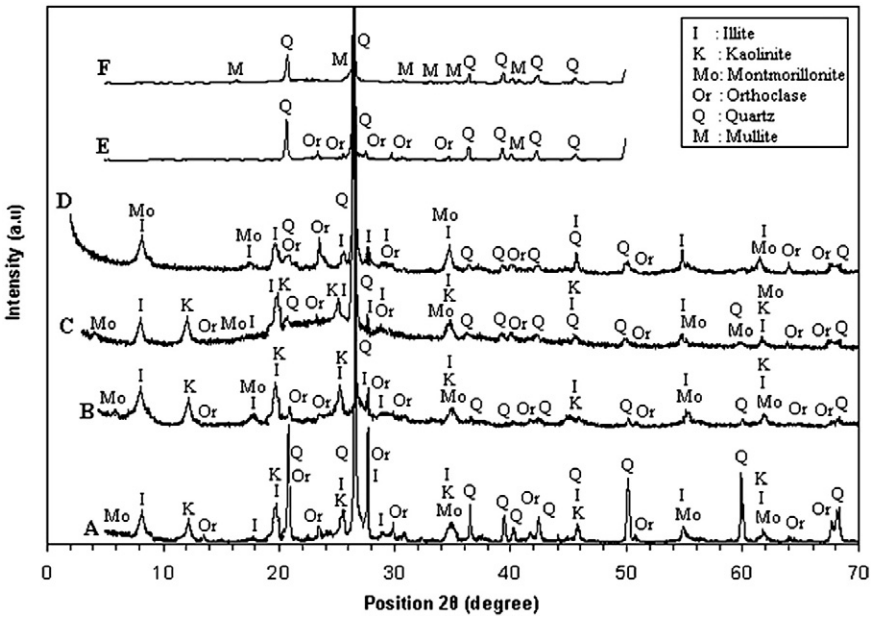

Fig. 3. X-ray diffraction patterns of raw AC (A), its oriented clay fraction (<2 μm) (B:untreated, C:glycolated, D:heated at 550 °C) and fired at 1100 °C (E) and 1200 oC (F).

procedure involving measuring mass differences between the as-fired and water saturated samples (immersed in boiling water for 2 h, cooling for 3 h and sweeping of their surface with a wet towel). The colour of the fired bodies (*Lab* values) was measured by the reflected light colorimeter (Konica Minolta Chroma Meter CR-400). *L* is a measure of lightness/darkness and varies from 100 for perfect white to 0 for absolute black. The red/green colour is indicated by *a*. The more positive is its value, the greater is the reddishness. More negative the greater the greenishness. Similarly, the yellow/blue is represented by *b*, positive value for yellow and negative for bluishness. The presenting results were the average of 10 tested specimens. The determination of water absorption and bending strength were carried out following the Turkish Standards (TS EN ISO 10545-3, 1995) and (TS EN ISO 10545-4, 1995).

To obtain a gresification diagram of the fired samples, the specimens were sintered in a fast-firing laboratory electric furnace between 800 and 1200 °C after drying at 110 °C.

3. Results and discussion

3.1. Mineralogical and chemical analysis

Figs. 3, 4, and 5 show the X-ray diffraction patterns of the raw clay samples (normal, fired at 1100 °C and 1200 °C) and their <2 μm clay fraction (untreated, glycoleted and heated to 550 °C) for AC and IC.

The following phases were identified for AC: illite as majority phases, kaolinite, montmorillonite, quartz and orthoclase; for IC: mostly kaolinite, illite, montmorillonite, and quartz (Table 2).

The reflections with d = 7.21 Å and 3.57 Å for the <2 μm fraction disappeared after heating to 550 °C. This confirms the presence of kaolinite which is transformed into metakaolinite above 450 °C in both clay samples. After glycol addition, the basal spacing of montmorillonite for IC and AC expanded from 14.3 Å to 16.4 Å and from 14.2 Å to 16.5 Å. The basal reflection of montmorillonite

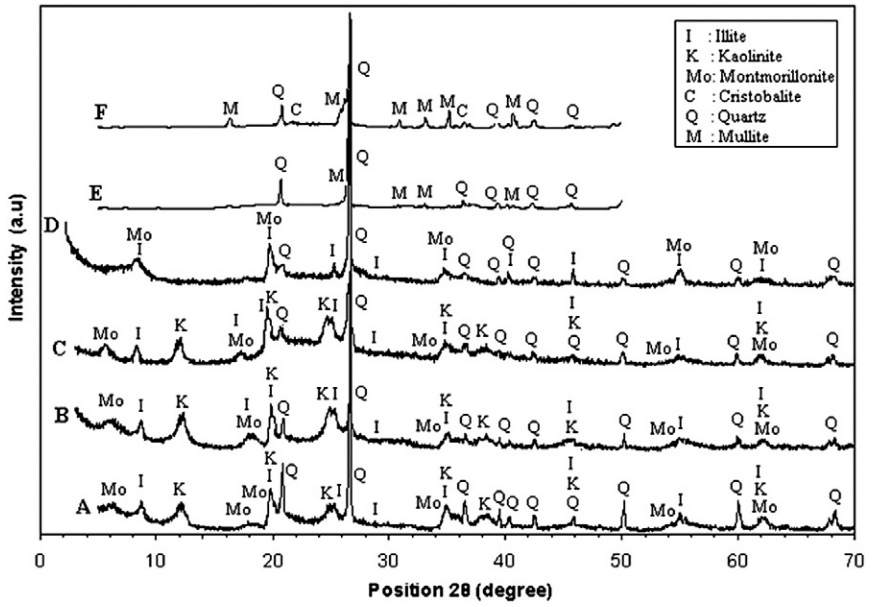

Fig. 4. X-ray diffraction patterns of raw IC (A), its oriented clay fraction (<2 μm) (B:untreated, C:glycolated, D:heated at 550 °C) and fired at 1100 °C (E) and 1200 °C (F).

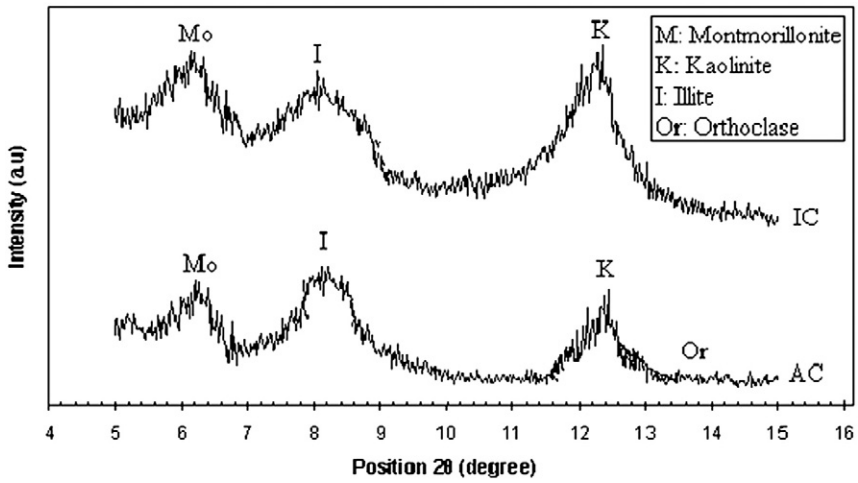

Fig. 5. XRD pattern between 5 and 15° 2θ (degree) of the <2 μm fraction of AC and IC.

collapsed to 10.8 Å for AC and 10.5 Å for IC after heating for 3 h at 550 °C.

The identified crystalline phases were in agreement with the results observed by XRF (Table 3). The presence of orthoclase in the <2 μm AC fraction is advantageous for densification. The sand fraction of AC, examined by microscope, was mainly composed of quartz, orthoclase and some agglomerated clay mineral particles.

The two clays consisted mainly of SiO_2 and Al_2O_3 which correspond to about 91% for AC and 82% for IC (Table 3) in agreement with the quantitative XRD analysis (Table 2). The amount of alkaline oxides (K_2O and Na_2O) that acting as flux materials was higher in AC (4.11%) than IC (2.11%) due to the relatively larger amount of illite and orthoclase. The low content of alkaline oxides in IC is a consequence of kaolinitic clays that naturally have a low content of flux materials (Monterio and Vieira, 2004). The amount of CaO and MgO was low for both clays and indicated the absence of carbonates. The high loss on ignition (10%) associated with low SiO_2 and high Al_2O_3 contents were due to the significant content of clay minerals in IC. The Fe_2O_3 content of AC was lower compared with IC. Besides its fluxing role, Fe_2O_3 also provides the fired products the characteristic reddish colour. However, Fe_2O_3 is not the only factor responsible for the coloration of ceramic wares, as also other constituents such as CaO, MgO, MnO and TiO_2 can appreciably modify the colour of fired clays (Kreimeyer, 1987). The temperature of firing, the amount of Al_2O_3 relative to a range of other constituents, and the furnace atmosphere all play an important role in the development of colour in the fired clay products (Fisher, 1984).

Typical X-ray diffraction patterns of the fired raw AC and IC samples at 1100 °C and 1200 °C are also given in Figs. 3, 4. All clay minerals (kaolinite, illite, and montmorillonite) of AC and IC disappeared by firing at 1100 °C while AC and IC formed mullite, IC also cristobalite at 1200 °C. Mullite was identified by the reflections at d = 5.41Å, 3.44 Å and 2.22 Å, and d = 5.43 Å, 3.40 Å and 2.22 Å, respectively. The mullite reflection intensity began to increase at 1200 °C, especially for IC. The orthoclase reflection of AC disappeared at 1200 °C according to its melting point (1170 °C). As expected, the intensity of the mullite reflections especially at 1200 °C was stronger for IC than AC, due to the higher kaolinite content in IC. Kaolinite is transformed into metakaolinite by removal of the hydroxyl groups of the silicate lattice above 450 °C (Yeskis, et al., 1985). As suggested previously by Okada et al. (1986), metakaolinite decomposes into spinel and an amorphous phase by firing. The reaction between the two phases produces mullite. Both the amorphous phase and mullite play an important role in the densification process (Baccour et al., 2008; Baccour et al., 2009). Different authors demonstrated that mullitisation can be enhanced by Fe^{+3}, supposedly by replacing Al^{+3} in the glass structure (Kamseu et al., 2007). The formation of mullite depends mainly on the type and proportion of kaolin used. Pure and well-crystallized kaolinite yields mullite at >1000 °C while disordered kaolinite forms mullite at >1200 °C (Sanchez, et al. 2001). The thermal transformation of illite to mullite was described previously by Wansard (1990) and Gonzalez-Garcia et al. (1990). Above 1100 °C, the amount of residual quartz decreased at higher temperature due to its dissolution and conversion of minor amounts into cristobalite. Cristobalite was not found in the fired products of AC because of the fluxing action of the interlayer cations of illite, which also inhibited the formation of cristobalite (Aras, 2004). Cristobalite from IC formed at 1200 °C was identified by the reflections at d = 4.06 Å and 2.49 Å.

3.2. Thermal analysis (DTA-TGA)

A significant endothermic peak at 111.3 °C for AC and 128 °C for IC (Figs. 6, 7) can be attributed to the removal of adsorbed and interlayer water of the clay minerals. The mass loss associated to this peak was about 7% and 1.2% for AC and IC. In addition, a large exothermic reaction between 200 and 400 °C was related to the decomposition of organic matter. A broad endothermic band centered at 560 °C for AC and 558 °C for IC was due to the dehydroxylation and the α→β-quartz transformation. The mass loss was 9.6% for IC and 2.2% for AC due to the high clay mineral content in IC.

An endothermic peak at 687 °C was attributed to dehydroxylation of montmorillonite in AC (Fig. 6). An exothermic peak was obtained at 915 °C and 945 °C for AC and IC due to the formation of the γ-Al_2O_3 spinel phase from metakaolinite (Brindley and Nakahira, 1959; Grim and Rowland, 2009; Khalfaoui et al., 2006; Okada et al., 1986;

Table 2
Mineral content of the raw clays and their <2 μm fraction (mass%) estimated by the computer program MAUD 1.9.

Samples	Kaolinite	Illite	Montmorillonite	Quartz	Orthoclase
AC (raw)	15.62 ± 0.72	33.67 ± 0.51	0.82 ± 0.02	41.85 ± 0.52	8.04 ± 0.18
AC (<2 μm)	31.22 ± 0.54	48.24 ± 0.87	3.36 ± 0.08	11.62 ± 0.10	5.54 ± 0.09
IC (raw)	49.22 ± 0.37	20.07 ± 0.85	1.26 ± 0.04	29.45 ± 0.49	–
IC (<2 μm)	55.50 ± 0.14	32.27 ± 0.98	4.58 ± 0.06	7.64 ± 0.08	–

Table 3
Chemical composition (mass%) of the clays and raw materials.

	SiO_2	Al_2O_3	Fe_2O_3	TiO_2	CaO	MgO	Na_2O	K_2O	SO_3	P_2O_5	LOI*	%
AC	77.66	13.76	1.04	0.06	0.17	0.17	0.10	4.01	0.23	–	2.80	100.00
IC	55.85	26.46	3.23	1.21	0.34	0.58	0.11	2.00	0.22	0.12	10.00	100.00
Albite	68.32	18.36	0.31	0.29	0.91	0.54	10.03	0.47	–	0.25	0.53	100.00
Altered gnays	77.16	13.39	0.77	0.16	1.00	0.42	4.42	0.77	–	0.10	1.76	100.00

*LOI = loss on ignition.

Srikrishna et al., 1990). Carthew (2009) pointed out that the DTA curve of well-crystallized kaolinite showed a slight endothermic peak immediately before the exothermic peak at around 980 °C due to the breakdown of the metakaolinite. The endothermic peak showed around 900 °C for IC (Fig. 7) just before the exothermic peak at 945 °C may demonstrate that the kaolinite in IC is well-crystallized in agreement with the XRD patterns. Finally, a small exothermic peak at 1078 °C for AC and 1122 °C for IC can be related to primary mullite crystallization as also indicated by the XRD patterns of fired clay samples (Figs. 3, 4). The more intense exothermic peak around 900 °C also indicated the higher kaolinite content in IC. Correspondingly, the total mass loss at 1200 °C was 12% for IC and 9.6% for AC.

3.3. Dilatometry

The dimensional changes observed after firing of the raw clays are given in Fig. 8.

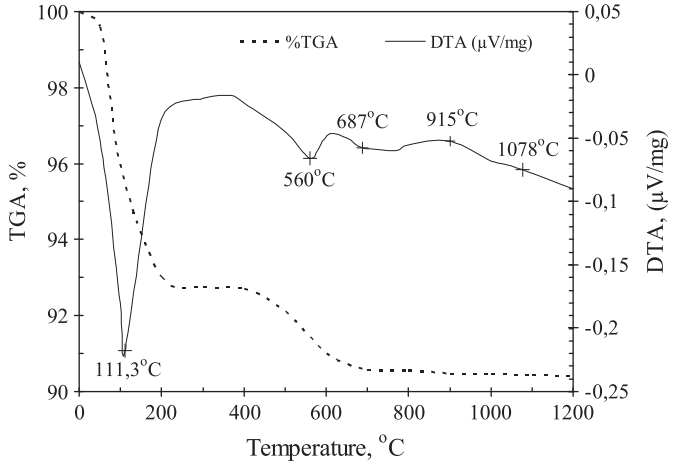

Fig. 6. DTA and DTG curves of Afyon clay.

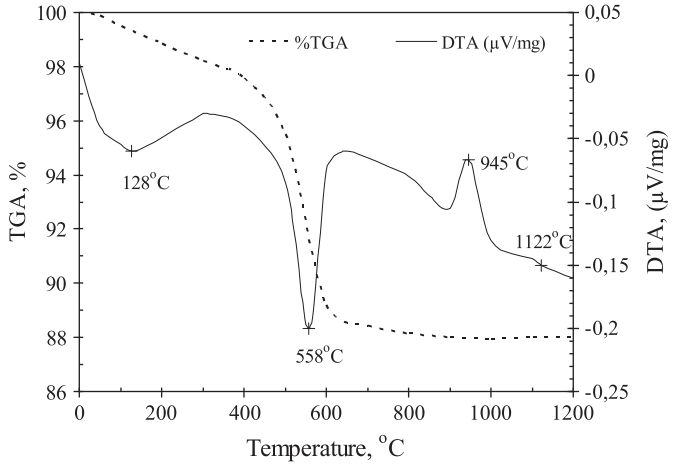

Fig. 7. DTA and DTG curves of Istanbul clay.

There was a small expansion (0.5%) up to 500 °C. This expansion was followed by larger changes between 500 and 600 °C due to the α→β-quartz transformation and between 600 and 952 °C due to β-quartz→β_2-tridymite transformation. Singer and Singer (1963) point out that α-quartz transformed into β-quartz at 573 °C with a volume increase of 2% and on further slow heating β-quartz changed to β_2-tridymite at 870 °C with a volume increase of 12%. The maximum expansion rate between 500 and 600 °C was 583 °C. The total expansion up to 952 °C was 1.6%. After a slight shrinkage starting at around 850 °C, a sharp shrinkage starting at 952 °C was attributed to sintering and the formation of vitreous phases. The maximum shrinkage rate between 952 and 1200 °C was obtained at 1071 °C. When the temperature reached 1200 °C, the shrinkage rate was about 3%. The total shrinkage between high temperature and room temperature was 4.8%.

The dilatometric curve of IC started with a slight expansion up to 110 °C due to desorption of adsorbed water. The shrinkage between 110 and 650 °C may be due to metakaolinite formation with

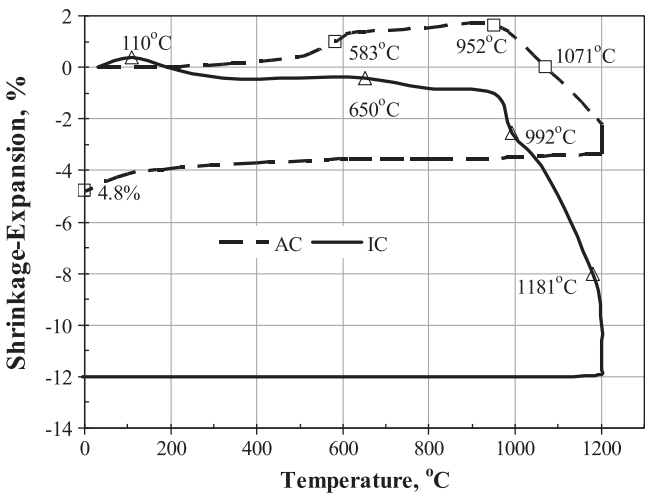

Fig. 8. Dilatometric curves of AC and IC.

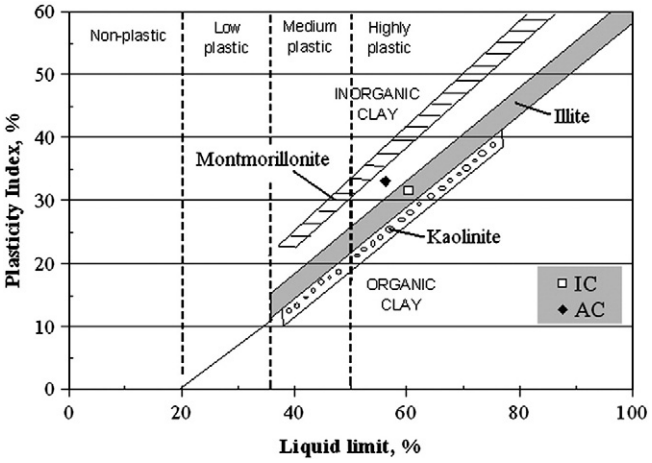

Fig 9. Location of AC and IC samples on the Casagrande chart.

Table 4
Fractional particle size distribution and Atterberg parameters of AC and IC.

	AC	IC
Liquid limit, mass%	56.1	60.3
Plastic limit, mass%	23.0	28.7
Plasticity index, mass%	33.1	31.6
>2000 μm	–	–
200–2000 μm	28.80	6.00
20–200 μm	4.99	4.91
2–20 μm	25.89	12.81
<2 μm	40.33	76.28
Total	100.00	100.00

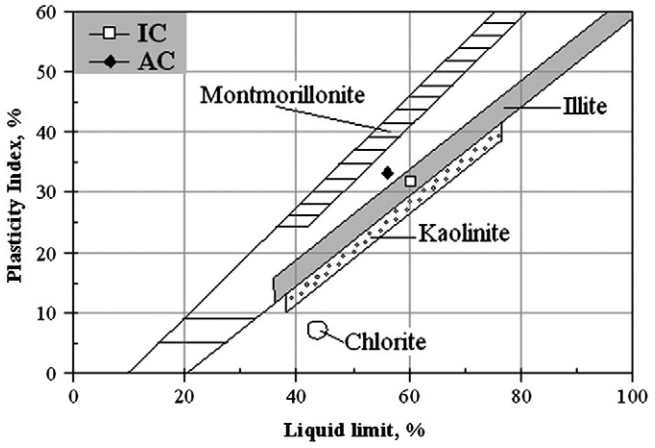

Fig 10. Position of AC and IC on the Holtz and Kovacs diagram.

concomitant loss of water (Souza et al., 2002). The second shrinkage between 650 and 800 °C can be attributed to sintering. A slight shrinkage starting at 800 °C and ending at around 950 °C was due to the formation of vitreous phases. The third shrinkage seen >950 °C was caused by the recrystallization of new ceramic phases and vitrification. The maximum shrinkage rate above 950 °C was observed at 1071 °C. The total shrinkage was 12%.

The smaller shrinkage of AC is related to higher content of quartz and illite compared to IC (Mahmoudi et al., 2008).

The dilatometry curves showed that between 850 and 952 °C for AC, and between 800 and 950 °C for IC the liquid phase was dominant. The higher content of K_2O in the AC raw material, especially in <2 μm fraction, may contribute to the rapid vitrification.

3.4. Evaluation of plasticity

Both clays presented similar plasticity. The plasticity index (PI) characterize them as highly plastic, which also demonstrated by Casagrande diagram (Fig. 9) (Table 4).

Both AC and IC samples also showed high values of PL. This is of importance for applications since it indicates the minimum moisture content necessary to reach a plastic condition. At a high plastic limit, the samples are more difficult to dry. On the other hand, the use of high plastic clays reduces the wearing down of the equipment for grinding and conformation (extruder). High plasticity is associated with bodies with greater mechanical strength (Monterio and Vieira, 2004). Fig. 10 shows the position of these clays on the Holtz and Kovacs diagram (Holtz and Kovacs, 1981).

Although IC had a higher clay fraction (<2 μm), the almost same PI value for both clays may be related to higher plastic limit of illite (35–60%) and montmorillonite (50–100%) than kaolinite (25–40%) (Mitchell, 1993).

3.5. Particle size analysis

The particle size distribution of clay is a factor in determining its suitability for various applications, and particular attention should be given to the finer fraction (lower than <2 μm) for ceramic products (Mahmoudi et al., 2008). AC presented a wider particle size distribution, with an average particle size of about 5 μm while the average particle size of IC was about 0.3 μm (Table 4, Fig. 11). The content of clay minerals (particles with sizes <2 μm) was about 76% for IC, whereas 40%

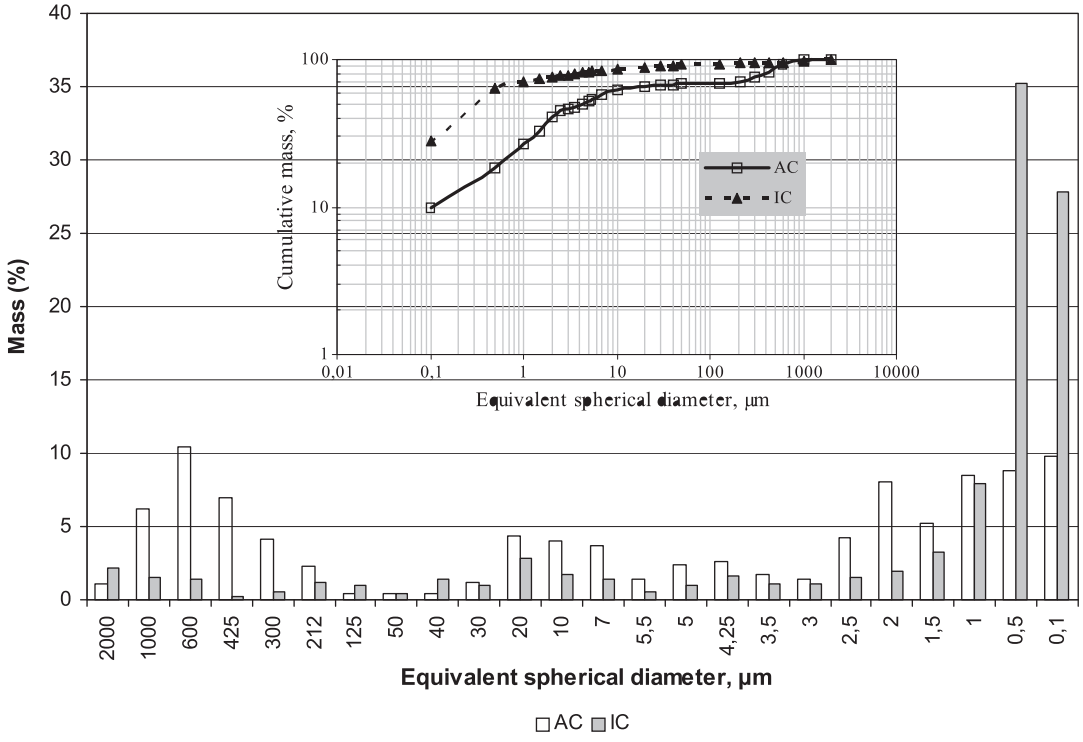

Fig. 11. Particle size distribution of AC and IC.

Table 5
Specific surface area and density of the clays.

	AC	IC	Kaolinite[a]	Illite[a]	Montmorillonite[a]
Specific surface area, m^2/g	38.52	39.10	10–20	65–100	50–800
Density	2.68	2.63	2.61	2.60	2.51

[a] Fang (1997).

Table 6
Formulation and parameters obtained from industrial tests.

		F_1	F_2	F_3	F_4	F_5
Formulations	IC	32	24	16	8	–
	AC	–	8	16	24	32
	Albite	32	32	32	32	32
	Altered gnays	36	36	36	36	36
IC/AC	For clay content of total 32%	4/0	3/1	2/2	1/3	0/4
Reological characteristics	Weight per liter, (g/lt)	1690	1687	1684	1680	1680
	Viscosity, sn	16	17	18	18	17
	Oversize fraction (>180 μm), %	2.80	2.80	2.85	2.86	2.85
Drying characteristics	Bending strength, N/mm^2	1.95	1.93	1.86	1.79	1.79
	Shrinkage, %	−0.2	+0.1	+0.0	+0.2	+0.2
Firing characteristics	Water absorption, %	3.32	3.35	3.70	3.72	3.85
	Bending strength, N/mm^2	35.3	35.0	34.3	33.5	33.3
	Shrinkage, %	7.56	7.02	5.74	5.10	4.16
Colour values	L	58.70	58.76	59.91	60.12	60.22
	a	4.27	4.21	4.06	3.77	3.73
	b	16.45	16.35	15.33	15.20	15.01

for AC. The silt fraction (particles with sizes between 2 and 20 μm) was about 13% for IC and 26% for AC. The sand fraction (particles with sizes >20 μm) was about 11% for IC and 34% for AC. The problem arising by the presence of particles in the coarse sand fraction (200–2000 μm) can be solved simply by grinding.

3.6. Specific surface area and density

Since the IC had a finer particle size distribution than AC, it was expected that the differences of specific surface areas of between IC and AC was more than the measured surface areas. As the specific surface area of kaolinite is usually smaller compared to illite (Ferrari and Gualtieri, 2006), the surface areas of the studied clays were almost the same. The density of the raw clay AC was slightly higher than that of IC, possibly due to the presence of orthoclase (Table 5).

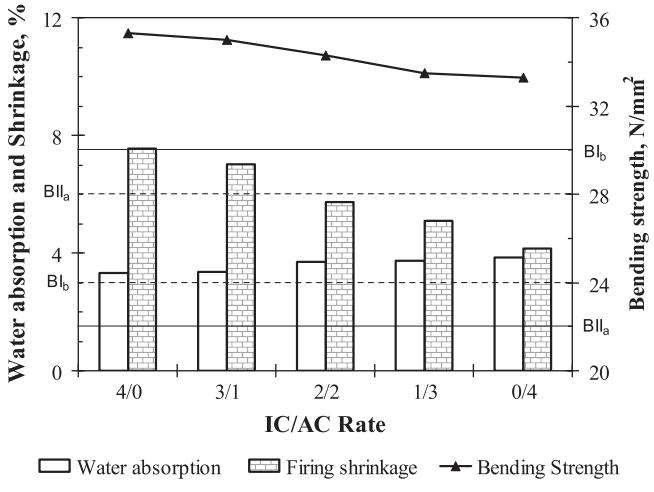

Fig. 12. Firing characteristics of formulated mixtures as a function of IC/AC proportions. The horizontal dashed lines are the limits of water absorption while the straight lines are the limits of bending strength corresponding to the TS EN 14411 standard groups.

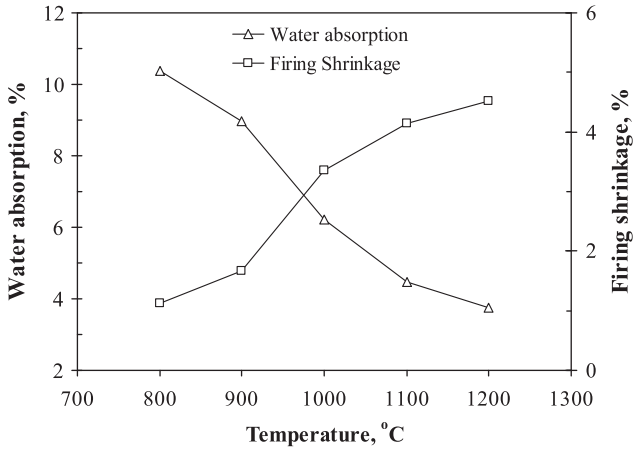

Fig. 13. Gresification diagram of fired samples of AC.

3.7. Industrial tests

All recipes had almost the same drying shrinkage (Table 6). A value of drying shrinkage between 0 and 0.5% is required to avoid microcracks around sand grains (Baccour et al., 2008).

The values of water absorption, firing shrinkage and firing bending strength were related to the IC/AC mass ratio in the clay fraction (32%). Water absorption was not distinctly changed (Fig. 12) when IC was substituted by AC.

The water absorption is the parameter according to Turkish Standards TS EN 14411 (2006), and it defines the class to which the tile products belong. The bodies showed values corresponding to class BII_a. The firing shrinkage decreased from 7.56% for F_1 with increasing amount of AC to 4.16% for F_5. This may be due to the higher quartz content in AC and the higher clay content in IC. The firing bending strength decreased with increasing proportions of AC. Higher mullite formation improved mechanical properties of composition with high amounts of IC.

All mixtures had almost same value of whiteness (L). In all recipes a and b was positive indicating that the colour tending to red and yellow. The increased redness and yellowness from F_5 to F_1 can be attributed to more amount of some oxide impurities, such as iron and titanium minerals in IC than AC (Table 3).

The sintering behaviour of the AC (Fig. 13) and IC (Fig. 14) was evaluated by the gresification diagram which presents the variation in properties of a ceramic body as a function of firing temperature.

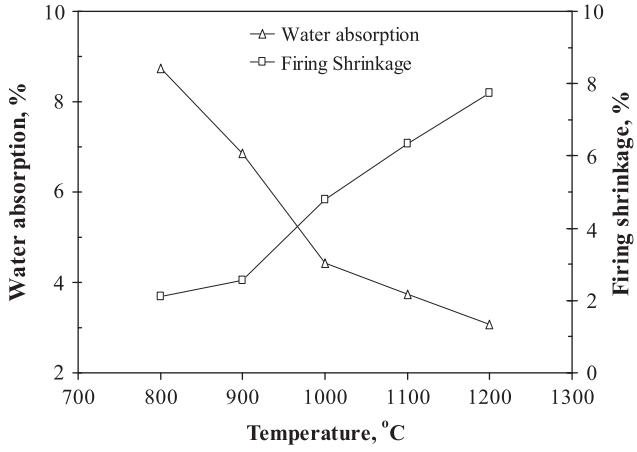

Fig. 14. Gresification diagram of fired samples of IC.

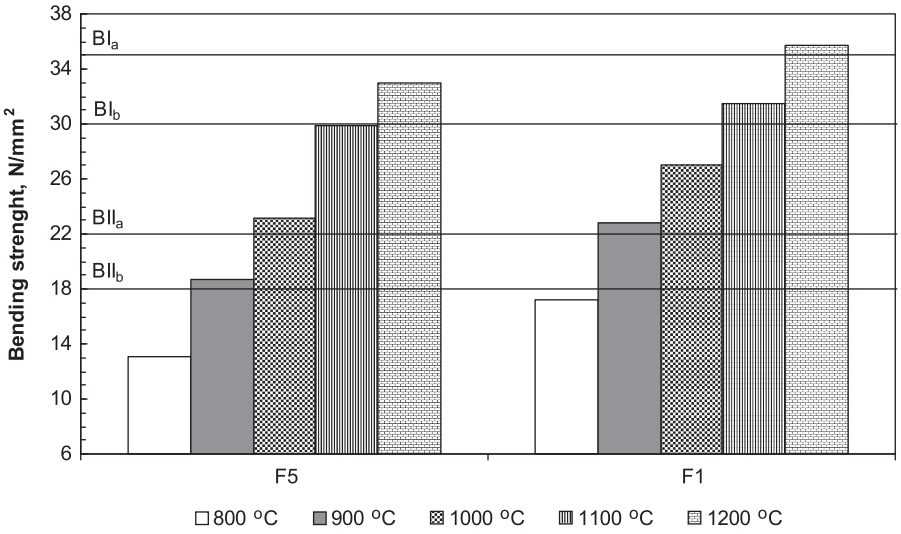

Fig. 15. Variation of bending strength with temperature for AC and IC. The horizontal straight lines are the limits of bending strength corresponding to the TS EN 14411 standard groups.

Above 900 °C, the values of water absorption decreased (Figs. 13, 14) and the amount of the liquid phase increased. This phase penetrates into the pores, closing them and isolating neighbouring pores. The liquid surface tension and capillarity help to bring pores closer together and reduce porosity. This explains the intense decrease of the water absorption in this temperature range (Baccour et al., 2009). The firing shrinkage up to 900 °C was small around 1.7% for AC and 2.5% for IC. Above 900 °C, the firing shrinkage ranged from 3.4 to 4.5% for AC.

The firing temperature had an important effect on the mechanical strength of ceramic tile (Fig. 15). The temperature increased the bending strength due to densification. As the liquid phase reduces the porosity, which hinders crack formation and improves the mechanical strength. Higher proportions of orthoclase in the <2 μm fraction of AC favoured vitrification and improved resistance of fired samples.

4. Conclusions

The clays from Afyon and Istanbul region, Turkey, were characterized by chemical, mineralogical and thermal analysis. The Afyon clay contained mainly illites and sand, the Istanbul clay kaolinite as the main component. There were no major differences in water absorption and bending strength when Istanbul clay was substituted gradually by Afyon clay in formulated floor tile bodies. The recipe composed of AC (formulation F_5) showed water absorption and bending strength values required for dry-pressed ceramic tile corresponding to class BII_a. The high content of alkali oxides and orthoclase in the <2 μm fraction of AC achieved a low level of water absorption >1000 °C. Afyon clay has qualities necessary for the manufacture of ceramic floor tiles, and it is an alternative ceramic raw material for the growing Turkish ceramic tile industry.

References

Ancey, C., 2007. Plasticity and geophysical flows: a review. J. Non-Newtonian Fluid Mech. 142 (1–3), 4–35.

Aras, A., 2004. The change of phase composition in kaolinite and illite rich clay based ceramic bodies. Appl. Clay Sci. 24, 257–269.

Baccour, H., Medhioub, M., Jamoussi, F., Mhiri, T., Daoud, A., 2008. Mineralogical evaluation and industrial applications of the Triassic clay deposits, Southern Tunisia. Mater. Charact. 59, 1613–1622.

Baccour, H., Medhioub, M., Jamoussi, F., Mhiri, T., 2009. Influence of firing temperature on the ceramic properties of Triassic clays from Tunisia. J. Materials Processing Technology 209 (6), 2812–2817.

Brindley, G.W., Brown, G., 1980. Crystal Structures of Clay Minerals and their X-ray Identification. Mineralogical Society.

Brindley, G.W., Nakahira, M., 1959. The kaolinite–mullite reaction series: II. Metakolin. J. Am. Ceram. Soc. 42 (7), 314–318.

Brunauer, S., Emmett, P.H., Teller, E., 1938. J. Am. Chem. Soc. 60, 309.

Can, M.M., Ozcan, S., Ceylan, A., Firat, T., in Press. Effect of milling time on the synthesis of magnetite nanoparticles by wet milling. Materials Science and Engineering. Article 2010.

Carthew, A.R., 2009. The quantitative estimation of kaolinite by differential thermal analysis. Mineralogical Society of America. http://www.minsocam.org/ammin/AM40/AM40_107.pdf.

Casagrande, A., 1947. Plasticity chart for the classification of cohesive soils. Trans. Am. Soc. Civ. Eng. 783–811.

Celik, H., Erturk, O., Day, N., 2009. Characterization of the clay in the region of Afyon and investigation of its utilization in ceramic floor tile bodies. Proceedings of the 7th Industrial Mineral Symposium and Exhibition. 25–27 February 2009. Kusadası, Izmir, Turkey, pp. 1–7.

Chang, L.L.Y., 2002. Industrial Mineralogy: Materials, Processes, and Uses. Prentice Hall, Upper Saddle River, New Jersey.

de Modesto, C.O., Bernardin, A.M., 2008. Determination of clay plasticity: indentation method versus Pfefferkorn method. Appl. Clay Sci. 40, 15–19.

Fang, H.Y., 1997. Introduction to Environmental Geotechnology. CRC Press LLC, America, p. 105.

Ferrari, S., Gualtieri, A.F., 2006. The use of illitic clays in the production of stoneware tile ceramics. Appl. Clay Sci. 32, 73–81.

Fisher, P., 1984. Some comments on the color of fired clays. Ziegelindustrie Int. 37, 475–483.

Gonzalez-Garcia, F., Romero-Acosta, V., Garcia-Ramos, G., Gonzalez-Rodriguez, M., 1990. Firing transformation of mixtures of clays containing illite, kaolinite and calcium carbonate used by ornamental tile industries. Appl. Clay Sci. 5, 361–375.

Grim, R., 1960. Some applications of clay mineralogy. Am Mineral 45, 259–269.

Grim, R.E., Rowland, A.R., 2009. Differential thermal analysis of clay minerals and other hydrous materials Part 1. Mineralogical Society of America. http://www.minsocam.org/ammin/AM27/AM27_746.pdf.

Holtz, R.D., Kovacs, W.D., 1981. Kansas Geotechnical Survey, Current Research in Earth Science, Bulletin 244, part 3, The Relationship Between Geology and Landslide Hazards of Atchison, Kansas and Vicinity.

Kamseu, E., Leonelli, C., Boccaccini, D.N., Veronesi, P., Miselli, P., Pellacani, M.G.U.C., 2007. Characterization of porcelain composition using two china clays from Cameroon. Ceramic International 33, 851–857.

Khalfaoui, A., Kacim, S., Hajjaji, M., 2006. Sintering mechanism and ceramic phases of an illitic-chloritic raw clay. J. Eur. Ceram. Soc. 26 (1–2), 161–167.

Kreimeyer, R., 1987. Some notes on the firing color of clay bricks. Appl. Clay Sci. 2, 175–183.

Lutterotti, L., 2010. MAUD WEB, version 1.9. http://www.ing.unitn.it/~luttero/maud. 2010.

Mahmoudi, S., Srasra, E., Zargouni, F., 2008. The use of Tunisian Barremian clay in the traditional ceramic industry: optimization of ceramic properties. Appl. Clay Sci. 42, 125–129.

Mitchell, J.K., 1993. Fundamentals of Soil Behavior2nd edition. John Wiley & Sons.

Monterio, S.N., Vieira, C.M.F., 2004. Influence of firing temperature on the ceramic properties of clays from Campos dos Goytacazes, Brazil. Appl. Clay Sci. 27, 229–234.

MTA, 2010. General Directorate of Mineral Research and Exploration of Turkey. http://www.mta.gov.tr. 2010.

Murthy, V.N.S., 2003. Geotechnical Engineering: Principles and Practices of Soil Mechanics and Foundation Engineering. Published by Mercel Dekker, Inc, America, p. 53.

Okada, K., Otsuka, N., Ossaka, J., 1986. Characterization of spinel phase formed in the kaolinite–mullite thermal sequence. J. Am. Ceram. Soc. 69, 251–253.
Peters, J.F., 1991. Determination of undrained shear strength of low plasticity clays. International Journal of Rock Mechanics and Mining Science and Geomechanics Abstracts. 28 (1), 13.
Sanchez, H., Orts, M.J., Garcia-Ten, J., Cantavella, V., 2001. Porcelain tile composition: effect on the phase formation and end products. Am. Ceramic Soc. Bull 80 (6), 43–49.
Singer, F., Singer, S.S., 1963. Industrial Ceramics. Chapman and Hall Ltd, London, pp. 99–100.
Sousa, S.J.G., Holanda, J.N.F., 2005. Development of red wall tiles by the dry process using Brazilian raw materials. Ceramic International 31, 215–222.
Souza, G.P., Sanchez, R., de Holanda, J.N.F., 2002. Characteristics and physical–mechanical properties of fired kaolinitic materials. Ceramica 48 (306), 102–107.
Srikrishna, K., Thomas, G., Martinez, R., Corral, M.P., De Aza, S., Moya, J.S., 1990. Kaolinite–mullite reaction series: a TEM study. J. Mater. Sci. 25, 607–612.
TCF, 2009. Turkish Ceramics Federation, Ceramic Tile World Data. http://www.serfed.com/content_files/9ec9b_03_Ceramic_Tile_World_Data.xls. 2009.
Thorez, J., 1975. Phyllosilicates and minerals. A Laboratory Handbook for X-ray Analysis. Editions G. Lelote B 4820, Dison Belgique.
TS EN 14411, 2006. Ceramic Tiles—Definitions, Classification, Characteristics and Marking. Turkish Standards Institution.
TS EN ISO 10545-3, 1995. Ceramic tiles—Part 3: determination of water absorption, apparent porosity, apparent relative density and bulk density. Turkish Standards Institution.
TS EN ISO 10545-4, 1995. Ceramic tiles—Part 4: determination of modulus of rapture and breaking strength. Turkish Standards Institution.
Wansard, G., 1990. Effets de la temperature sur la composition mineralogique et sur la structure de la brique de Wanlin (Belgique). Bull. Soc. B Geol. 99, 207–219.
Yeskis, D., Koster, A., Guggenheim, S., 1985. The dehydroxylation of kaolinite. Am. Mineral 70, 159–164.